ISSN: 1999-6691, e-ISSN: 2782-3709 DOI: http://doi.org/10.7242/1999-6691/2024.17.1.1

.

Research article

Modeling of nanochannels in synthetic membranes

***M.S. Alekseev*[1,3], *R. R. Ponomarev*[2,3], *V.S. Shelistov*[3], *V.A. Popov*[2,3], *I.A. Morshneva*[2], *E.A. Demekhin*[3,4]**

[1] *Kuban State University, Krasnodar, Russian Federation*
[2] *Southern Federal University, Rostov-on-Don, Russian Federation*
[3] *Financial University under the Government of the Russian Federation, Moscow, Russian Federation*
[4] *Moscow State University, Research Institute of Mechanics, Moscow, Russian Federation*

The behavior of a diluted electrolyte in a system of joint microchannel and nanochannel with charged dielectric walls under the action of external potential difference and external pressure is investigated numerically. The surface charge on the nanochannel walls prevents the ions of corresponding polarity from passing through it. Consequently, the system in question acquires ion-selective properties and can, under certain assumptions, be viewed as a fragment of an ion-selective membrane, including one synthesized by creating nanopores in a dielectric material. Such systems are used in experiments to control the movement of charged particles through concentration polarization. The objective of the work is to investigate the influence of a single pore on electrolyte flow and the possibilities to control that flow by changing the geometric and physical properties of the pore. The investigation relies on the specially developed simplified models based on cross-section-averaged Nernst–Planck, Poisson and Stokes equations that are subsequently reduced to a single nonlinear differential equation. The simplified models allow identifying the impact of different physical mechanisms of electrolyte movement: pressure-based (generated by the external mechanical action) and electroosmotic (generated by the electric field). A finite-difference method with semi-implicit time integration is used for the numerical solution of equations. It has been found that the behavior of the system qualitatively matches the behavior of a cell based on a non-ideally-selective ion-exchange membrane. In particular, the model correctly predicts the underlimiting and limiting electric current regimes, as well as vortex formation near the nanochannel inlet due to concurrency between electrolyte movement mechanisms. The proposed models can be extended to describe a channel with arbitrary geometry and an electrolyte with arbitrary number of charged species.

Keywords: membrane, nanochannel, Nernst–Planck–Poisson–Navier–Stokes system, electroosmosis, numerical simulation

Received: 13.06.2023 / *Published online*: 01.04.2024

1. Introduction

Modern technological advances make it possible to create long nanochannels with characteristic cross sections of 10–100 nm and lengths on the order of several hundred microns. Such nanochannels (nanotubes) have a wide application [1–3]. One of the most important properties of nanochannels used in practice is their selectivity towards charged particles. The walls of the channels usually carry an electric charge. The electric field created by it prevents or hinders the passage of ions of the corresponding sign through the channel. A similar mechanism is characteristic of ion-selective membranes, which are essentially porous media with pore size on the order of tens of nanometers. The geometric and physicochemical properties of the pores have a significant influence on the behavior of membranes, and the manufacturing technology of the latter does not give full control over their properties, so before the membrane is used in a particular installation, it undergoes additional processing [4]. Optimal treatment is often achieved by trial and error. The integral properties of ion-selective membranes are well enough studied. For example, their current–voltage characteristic has three typical sections [5]: at low potential difference, the current through the membrane obeys Ohm's law (underlimiting regime), saturation of the current occurs at increasing potential difference (limiting regime), but then the current starts to increase again in proportion to the potential difference (overlimiting regime). The occurrence of the overlimiting regime is caused by a special type of instability [6] and, as shown by numerical modeling [7], is determined solely by the asymmetry of the ion flux, i.e., it does not qualitatively depend on the membrane microstructure. As a consequence, in many theoretical works, the membrane is represented as a homogeneous (or, less often, piecewise homogeneous) object with specified properties. At the same time, similar instabilities also arise in the vicinity of specially fabricated nanochannel systems [8]; therefore, the question of which of the manifested ion properties are systemic and which are provided by a single nanochannel is of particular interest. In the future, the fabrication of a system of nanochannels with specially selected properties could become an alternative to the use of traditional membranes.

The electrolyte flow in membranes is usually described by the Poisson and Darcy equations [9–11]. In sufficiently wide channels, an approach based on the assumption of electroneutrality of the electrolyte outside thin (up to 100 nm) Debye layers is used [12]. For the nanochannels discussed above, this assumption may be violated, resulting in the need to solve the full nonlinear system of the Nernst-Planck, Poisson, and Navier-Stokes equations [13], which is computationally

complex in the case of nontrivial channel geometry. The problem of flow in nanochannels was solved numerically in the full formulation in [14, 15], where "concentration jumps" resembling shock waves of gas dynamics were found. The obtained result has both fundamental (especially for mechanics, as a manifestation of a typical feature of nonlinearity) and practical significance (the papers suggest that when adding third-type ions to the electrolyte, their strong concentration is possible in these jumps). On the other hand, the proposed approach has limitations related to the resource-intensive calculations for nanochannels, the length of which is many times greater than their width.

There are approaches [16, 17] based on a weakly nonlinear approximation, in which many restrictions are introduced to simplify the problem, e.g., weak nonlinearity, small Debye numbers. In addition, the model [17] does not take into account the advective mechanism of ion transport: only diffusion and electromigration are taken into account. The results of these works also poorly agree with the results of [14, 15].

In this paper, a simplified model based on the cross-sectionally averaged Nernst-Planck, Poisson, and Navier-Stokes equations in the creeping flow approximation is studied. The changes along the nanochannels are considered to be slower than in the transverse direction. As a consequence, it is possible to introduce a small parameter for the asymptotic approach and to perform averaging without assuming weak nonlinearity and other oversimplifying assumptions. The electrolyte behavior is considered in a system of coupled microchannel and nanochannel with plane-parallel walls. Such geometry, on the one hand, corresponds to the accepted assumption (except for the junction vicinity), and on the other hand, allows to qualitatively compare the modeling results with the data obtained by others, e.g., [15]. The junction region also, albeit roughly, depicts the surface of the ion exchange membrane in the vicinity of one of the pores, which makes it possible to qualitatively compare the results with the behavior of membranes. In particular, the system under consideration is expected to have underlimiting and limiting regimes, but not the overlimiting one, which in practice arises due to vortex formation near the selective surface [6], and the characteristic vortex size is many times larger than the pore size [18]. The validity of the model is additionally checked by comparison with the numerical solution of the unsimplified equations.

2. Problem statement

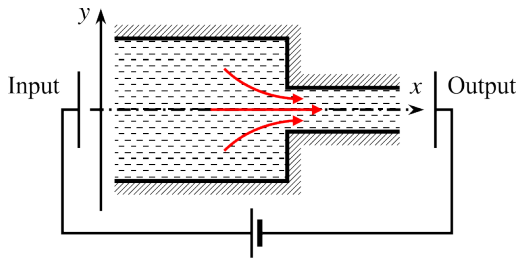

Fig. 1. Schematic representation of the problem geometry

The flow of a symmetric univalent binary electrolyte in a system consisting of a rectangular nanopore extending into a rectangular micropore (Fig. 1) under the joint action of potential difference and pressure is considered. The pore walls are impermeable and are assumed to be uniformly charged. The size of the nanopore is assumed to be large enough for the continuity hypothesis to apply to the flow. In this case, the electrolyte motion is described by the equations:

$$\begin{aligned} &\frac{\partial \tilde{c}^+}{\partial \tilde{t}} + \tilde{\nabla}\cdot\tilde{\mathbf{j}}^+ = 0, \quad \tilde{\mathbf{j}}^+ = \tilde{\mathbf{U}}\tilde{c}^+ - \frac{\tilde{D}\tilde{F}}{\tilde{R}\tilde{T}}\tilde{c}^+\tilde{\nabla}\tilde{\Phi} - \tilde{D}\tilde{\nabla}\tilde{c}^+, \\ &\frac{\partial \tilde{c}^-}{\partial \tilde{t}} + \tilde{\nabla}\cdot\tilde{\mathbf{j}}^- = 0, \quad \tilde{\mathbf{j}}^- = \tilde{\mathbf{U}}\tilde{c}^- + \frac{\tilde{D}\tilde{F}}{\tilde{R}\tilde{T}}\tilde{c}^-\tilde{\nabla}\tilde{\Phi} - \tilde{D}\tilde{\nabla}\tilde{c}^-, \end{aligned} \tag{1}$$

$$\tilde{d}\tilde{\nabla}^2\tilde{\Phi} + \tilde{F}\left(\tilde{c}^+ - \tilde{c}^-\right) = 0, \tag{2}$$

$$-\tilde{\nabla}\tilde{P} + \tilde{\mu}\tilde{\nabla}^2\tilde{\mathbf{U}} = \tilde{F}\left(\tilde{c}^+ - \tilde{c}^-\right)\tilde{\nabla}\tilde{\Phi}, \quad \tilde{\nabla}\cdot\tilde{\mathbf{U}} = 0, \tag{3}$$

where (1) — Nernst-Planck equations for ion transport, (2) — Poisson equation for electric potential distribution, (3) — Navier-Stokes equations for liquid phase flow. The latter, due to the smallness of characteristic scales, are conveniently taken in the creeping flow approximation. In (1)–(3), the following notations are adopted: $\tilde{c}^{\pm}$ — concentrations of cations and anions; $\tilde{t}$ — time; $\tilde{\mathbf{U}}$ — velocity vector; $\tilde{D}$ — diffusion coefficient of cations and anions; $\tilde{F}$ — Faraday constant; $\tilde{R}$ — universal gas constant; $\tilde{T}$ — absolute temperature; $\tilde{\Phi}$ — electric potential; $\tilde{d}$ — dielectric constant; $\tilde{P}$ — pressure; $\tilde{\mu}$ — dynamic viscosity. Hereinafter, dimensional quantities are marked with a tilde. Temperature, dielectric permittivity, and viscosity are assumed constant in the considered formulation. The following conditions are set on the pore walls:

– no-slip condition

$$\tilde{\mathbf{U}} = \mathbf{0}; \tag{4}$$

– wall impermeability to ions

$$\tilde{\mathbf{j}}^+\cdot\mathbf{n} = \tilde{\mathbf{j}}^-\cdot\mathbf{n} = 0; \tag{5}$$

– a potential jump

$$\tilde{d}\tilde{\nabla}\tilde{\Phi}\cdot\tilde{\mathbf{n}}=-\tilde{\sigma}, \tag{6}$$

where $\mathbf{n}$ is the external unit normal to the pore surface, and $\tilde{\sigma}$ is the surface charge density. An electroneutral solution with ion concentrations of $\tilde{c}^+=\tilde{c}^-=\tilde{c}_0$ is supplied to the inlet. The inlet velocity is assumed to have a Poiseuille profile corresponding to a given pressure difference, and the potential is assumed to be constant and this value is taken to be zero, $\tilde{\Phi}=0$. Soft conditions for concentrations and velocities are placed at the outlet of the nanochannel:

$$\frac{\partial\tilde{c}^+}{\partial\tilde{x}}=\frac{\partial\tilde{c}^-}{\partial\tilde{x}}=0;$$

$$\frac{\partial\tilde{U}_x}{\partial\tilde{x}}=\tilde{U}_y=0,$$

and the potential corresponds to the given potential difference: $\tilde{\Phi}=\Delta\tilde{V}$.

The distribution of ion concentrations at the initial moment of time is assumed to be uniform:

$$\tilde{c}^+=\tilde{c}^-=\tilde{c}_0.$$

Strictly speaking, the electrolyte will not preserve electroneutrality in a channel with charged walls, and it would be more correct to use the stationary solution of the problem for the case of the absence of an external field and pressure difference (obtained, for example, by the establishment method from the above problem with an electroneutral initial state) as the initial condition. However, the subsequent calculations showed that in the process of evolution the difference between these initial conditions decreases rapidly, so, to simplify the algorithm, the establishment stage is skipped.

All quantities are reduced to a dimensionless form. The following quantities are taken as characteristic ones: for length — half of the channel width at the outlet $\tilde{h}_0$; for velocity — $\tilde{D}/\tilde{h}_0$; for time — $\tilde{h}_0^2/\tilde{D}$; for dynamic quantity — $\tilde{\mu}$. The concentrations of cations and anions are referred to $\tilde{c}_0$; the characteristic potential is the thermal potential $\tilde{\Phi}_0=\tilde{R}\tilde{T}/\tilde{F}$. The dimensionless equations (1)–(3) are as follows:

$$\begin{aligned}&\frac{\partial C^+}{\partial t}+\nabla\cdot\mathbf{j}^+=0,\quad \mathbf{j}^+=\mathbf{U}C^+-C^+\nabla\Phi-\nabla C^+,\\ &\frac{\partial C^-}{\partial t}+\nabla\cdot\mathbf{j}^-=0,\quad \mathbf{j}^-=\mathbf{U}C^-+C^-\nabla\Phi-\nabla C^-,\end{aligned} \tag{7}$$

$$2\varepsilon^2\nabla^2\Phi=C^--C^+, \tag{8}$$

$$\nabla^2\mathbf{U}=\nabla P-\kappa\nabla\Phi\nabla^2\Phi,\quad \nabla\mathbf{U}=0. \tag{9}$$

Here $\varepsilon=\tilde{\lambda}_D/\tilde{h}_0$, $\tilde{\lambda}_D=\sqrt{\tilde{d}\tilde{\Phi}_0/(2\tilde{c}_0\tilde{F})}$ — Debye length, $\kappa=\tilde{d}\tilde{\Phi}_0^2/(\tilde{\mu}\tilde{D})$ — a coupling coefficient of hydrodynamic and electrostatic quantities.

The boundary conditions (4)–(6) transform into the following:

$$\mathbf{U}=\mathbf{0}, \tag{10}$$

$$\mathbf{j}^+\cdot\mathbf{n}=\mathbf{j}^-\cdot\mathbf{n}=0, \tag{11}$$

$$\varepsilon\nabla\Phi\cdot\mathbf{n}=-\sigma. \tag{12}$$

The charge density in equation (12) is normalized by a value $\tilde{\sigma}_0=\tilde{d}\tilde{\Phi}_0/\tilde{h}_0$, naturally derived from the above transformations. At the initial moment of time ($t=0$) the dimensionless concentrations are equal to unity:

$$C^+=C^-=1.$$

The condition for the inlet concentrations takes the same form. The condition for the outlet is written as

$$\frac{\partial C^+}{\partial x}=\frac{\partial C^-}{\partial x}=0.$$

The conditions for the potential and velocities remain as they are and for the sake of brevity are not given.

3. Solution methodology

The system (7)–(12) can be directly solved numerically, but in this case its solution is rather resource-intensive. To simplify the formulation, we assume that the length of the micropore is much larger than its width and the changes in the tangential direction are much slower than in the normal one, $\partial/\partial x \ll \partial/\partial y$. We neglect the violation of this condition in a small neighborhood of the junction (see [14] and the literature cited there for a brief justification of such neglection). This makes it possible to use an integral method like the Karman-Polhausen method [19]: in equations (8), (9) we ignore the tangential derivatives and find analytic solutions (8), (9) with an explicit dependence on the coordinate y, while the equations (7) are to be integrated over y in order to find the dependence on x. Two simplifying approaches will be presented below: the well-known Gouy–Chapman approach, which is valid for small Debye numbers ($\varepsilon \ll 1$) and an approach based on the assumption of smallness of the surface charge ($\sigma \ll 1$). These approaches are independent. Small σ allows one to consider any values of ε, including sufficiently large ones (of course, if they do not go beyond the boundaries of applicability of the continuum hypothesis), and vice versa. It can be assumed that each of these approaches will reduce the selectivity of the channel with respect to ions of different signs: ions with the charge identical to the walls will not encounter appreciable resistance from the electrostatic forces either because of the initial smallness of the wall charge or because of the weakening of the field created by them to the middle of a sufficiently wide (at $\varepsilon \ll 1$) channel.

Let us analyze the simplification approaches in more detail. Let us consider the system shown in Figure 1 as a channel of variable cross-section (Fig. 2). Let us define the wall profile by the function $y = \pm H(x)$, which is piecewise constant because it undergoes a discontinuity at the junction of micro- and nanopores. For convenience, it can be approximated by a smooth function with a sharp change in a small neighborhood of the junction (the specific form of this function will be given in the description of the numerical method). At first, neglecting small changes of the potential in the tangential direction, we reduce the Poisson equation (8) to the form:

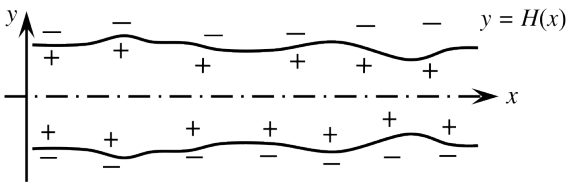

Fig. 2. An axisymmetric channel of variable cross-section with charged walls

$$2\varepsilon^2 \frac{\partial^2 \Phi}{\partial y^2} = C^- - C^+. \tag{13}$$

For the case $\sigma \ll 1$, equation (13) has a solution:

$$\Phi = \frac{\sigma \cosh\left(y\sqrt{C}/\varepsilon\right)}{\sqrt{C}\sinh\left(H\sqrt{C}/\varepsilon\right)}, \quad C^+ = C\left(1 - \frac{\sigma \cosh\left(y\sqrt{C}/\varepsilon\right)}{\sqrt{C}\sinh\left(H\sqrt{C}/\varepsilon\right)}\right), \quad C^- = C\left(1 + \frac{\sigma \cosh\left(y\sqrt{C}/\varepsilon\right)}{\sqrt{C}\sinh\left(H\sqrt{C}/\varepsilon\right)}\right), \tag{14}$$

where C is a slowly varying function of the variables x and t: $C = C(x,t)$. For $\varepsilon \ll 1$, the solution of equation (13) is as follows

$$C^- = C\left[\frac{2}{1 - T\exp\left((y-H)\sqrt{C}/\varepsilon\right)}\right]^{+2}, \quad C^+ = C\left[\frac{2}{1 - T\exp\left((y-H)\sqrt{C}/\varepsilon\right)}\right]^{-2}, \tag{15}$$
$$\Phi = 4\operatorname{arcth}\left[T\exp\left((y-H)\sqrt{C}/\varepsilon\right)\right]$$

and is valid at $0 < y < H$; the function $T(x,t)$ is of the form:

$$T = -\sqrt{1 + \left(\frac{2\sqrt{C}}{\sigma}\right)^2} - \frac{2\sqrt{C}}{\sigma}.$$

It follows from the continuity equation $\partial U/\partial x + \partial V/\partial y = 0$ at $\partial/\partial x \ll \partial/\partial y$ that the normal component of velocity V is small compared to the tangential component U: $V \ll U$. Accordingly, the Stokes equations (9) are reduced to a single equation:

$$\frac{\partial^2 U}{\partial y^2} = \frac{\partial P}{\partial x} + \kappa \frac{\partial^2 \Phi}{\partial y^2} E. \tag{16}$$

Since the tangential electric field strength $E \equiv -\partial\Phi/\partial x$, which arises in equation (16), depends significantly on the external field, it is considered as an unknown function to be determined later. On the other hand, in the term $\partial^2\Phi/\partial y^2$ this

dependence is small, so we can substitute there the value of Φ found from (14) or (15). In the subsequent formulas, Φ will mean this asymptotic value rather than the full electric potential.

The tangential velocity U is a rapidly varying function of y but a slowly varying function of x (and t). Let us represent U as a superposition of the pressure (U_p) and electroosmotic (U_e) parts, each satisfying the boundary conditions of y. Then equation (16) is decomposed into two:

$$U_p=\frac{1}{2}\frac{\partial P}{\partial x}\left(y^2-H^2\right),\quad U_e=\kappa E(\Phi-\zeta). \tag{17}$$

Here ζ is the value of the potential Φ on the walls $y=\pm H$, which at $\varepsilon\ll 1$ acquires the physical value of the zeta potential.

The pressure and electroosmotic parts of the velocity create the corresponding flow rates along the channel cross-section. Due to the symmetry of the problem, it is convenient to consider halves of these flow rates, respectively Q_p and Q_e:

$$Q_p=-\frac{\partial P}{\partial x}\cdot\frac{H^3}{3},\quad Q_e=\kappa E\int\limits_0^H(\Phi-\zeta)dy. \tag{18}$$

For physical reasons, we require that the total half-flow rate $Q=Q_p+Q_e$ is independent of x. This condition allows us to express the unknown function $\partial P/\partial x$ in the relation (18) through the unknown constant Q:

$$\frac{\partial P}{\partial x}=\frac{3}{H^3}\left(\kappa E\int\limits_0^H(\Phi-\zeta)dy-Q\right). \tag{19}$$

Then, taking into account (19), U_p in the relation (17) will take the following form:

$$U_p=\frac{3}{2H^3}\left(Q-\kappa E\int\limits_0^H(\Phi-\zeta)dy\right)\left(H^2-y^2\right).$$

Now let us integrate the ion transport equations (7). Taking advantage of the conditions of wall impermeability for both types of ions and interchanging the differential operators and the integrals, we obtain:

$$\frac{\partial}{\partial t}\int\limits_0^H C^{\pm}dy+\frac{\partial}{\partial x}\int\limits_0^H UC^{\pm}dy\pm\frac{\partial}{\partial x}E\int\limits_0^H C^{\pm}dy=\frac{\partial^2}{\partial x^2}\int\limits_0^H C^{\pm}dy-\frac{\partial}{\partial x}\left(\frac{\partial H}{\partial x}\,C^{\pm}\Big|_{y=0}^{y=H}\right). \tag{20}$$

Substituting the solutions found above into (20) allows us to obtain equations with respect to the two unknown functions, C and E, and to the parameter Q. We will omit the corresponding derivations, but point out that subtraction of equation (20), written for C^-, from equation (20) for C^+ leads to annihilation of the derivative by t, and the remaining ordinary differential equation after a single integration by x turns into an algebraic equation. At $\sigma\ll 1$, the final equation takes the form:

$$\frac{\partial}{\partial t}(HC)+\frac{\partial}{\partial x}(QC-\varepsilon\sigma E)=\frac{\partial}{\partial x}\left(H\frac{\partial C}{\partial x}\right), \tag{21}$$

where $E=M/N$, and M and N are given by the relations

$$M=\frac{6Q\varepsilon^2}{H^3}\left(\zeta H-\frac{\varepsilon\sigma}{C}\right)+2\zeta C\frac{\partial H}{\partial x}+I,\quad N=-\frac{6\kappa\varepsilon^2}{H^3}\left(\zeta H-\frac{\varepsilon\sigma}{C}\right)^2+\kappa\left(\sigma^2H+\varepsilon\sigma\zeta-CH\zeta^2\right)+2CH. \tag{22}$$

The quantity I in (22) is the integration constant, which has the physical meaning of the electric current flowing through the channel.

The case of $\varepsilon\ll 1$ produces a more complicated equation that contains a special function — the dilogarithm $\mathrm{Li}_2(\pm T)$:

$$\frac{\partial}{\partial t}\left[2HC+4\varepsilon\sqrt{C}\left(\sqrt{1+\frac{\sigma^2}{4C}}-1\right)\right]-\kappa\frac{\partial}{\partial x}\left\{E\zeta\left[2HC+4\varepsilon\sqrt{C}\left(\sqrt{1+\frac{\sigma^2}{4C}}-1\right)\right]\right\}+$$
$$+\frac{\partial}{\partial x}\left\{\frac{3}{H^3}Q_p\left[\frac{2}{3}CH^3-4\varepsilon^2\ln\left(1-T^2\right)-\frac{4\varepsilon^3}{\sqrt{C}}\left(\mathrm{Li}_2(1-T)+\mathrm{Li}_2(1+T)\right)\right]\right\}+$$

$$+4\varepsilon\kappa\frac{\partial}{\partial x}\left\{E\sqrt{C}\left[\mathrm{Li}_2(1-T)-(1+T)-\frac{4T}{1-T^2}+\zeta\frac{1+T^2}{1-T^2}\right]\right\}-2\varepsilon\frac{\partial}{\partial x}(\sigma E)=$$
$$=\frac{\partial^2}{\partial x^2}\left[2HC+4\varepsilon\sqrt{C}\left(\sqrt{1+\frac{\sigma^2}{4C}}-1\right)\right]-\frac{\partial}{\partial x}\left\{\left(\sigma^2+2C\right)\frac{\partial H}{\partial x}\right\}, \tag{23}$$

where Q_p and ζ are defined through the potential given by the formula (15). The functions M and N, through which E is found, will have a form structurally similar to (22), which for the sake of brevity is not given here. For the simplified equations (21) and (23), the role of boundary conditions for potential and velocity is played by two parameters: current I and flow rate Q. Note that these parameters can be replaced by the potential difference ΔV and pressure difference ΔP, respectively:

$$\Delta V=\int_0^L E dx, I=\left(\Delta V-\int_0^L\frac{M-I}{N}dx\right)\Big/\int_0^L\frac{dx}{N},$$
$$\Delta P=\int_0^L\frac{\partial P}{\partial x}dx,\quad Q=\left(\int_0^L\frac{3\kappa E}{H^3}\int_0^H(\Phi-\zeta)dydx-\Delta P\right)\Big/\int_0^L\frac{3}{H^3}dx,$$

where L is the dimensionless channel length. In the calculations described below, the pair ΔV and Q was supplied, unless explicitly stated otherwise. A numerical method based on finite-difference approximation was developed to solve the obtained equations, both the full system (7)–(12) and its simplifications (21) and (23). The spatial derivatives were given by second-order central differences on staggered grids, and a semi-implicit Runge-Kutta method of third-order accuracy was used for time integration [20]. The Jacobian of the numerical operator was considered as the implicit part. To control the accuracy of the method, the number of grid nodes was doubled, and to control the influence of boundary conditions, the channel length was doubled (with simultaneous doubling of the potential difference in order to keep the mean field strength constant).

The equations (8), (9) in the unsimplified formulation were solved by a direct method, essentially reduced to the solution of systems of linear algebraic equations. The rectangular geometry allows us to set the boundary conditions explicitly, without using the method of immersed boundaries. To reduce the computational complexity of the solution, eigenfunction decomposition and splicing of solutions at the junction of microchannel and nanochannel were used. This technique reduced the solution of a linear system with a sparse matrix to a multiple application of a modified tridiagonal matrix algorithm. Nevertheless, due to the stiffness of the system of equations, the performance of such an algorithm turned out to be insufficient, so it was used mainly for verification of the results obtained in the simplified approach.

4. Modeling results

The calculations were performed in a channel with a given profile

$$H(x)=\frac{1+R}{2}+\frac{1-R}{2}\mathrm{th}\left[\gamma\left(x-\frac{L}{2}\right)\right],$$

which simulates the junction of a microchannel of width R and a nanochannel of width 1 at $x=L/2$. The values of $L=1000$, $R=1000$, $\gamma=1$ were taken. The $\kappa=0.26$ corresponding to potassium chloride solution was taken; the wall charge density was assumed constant for simplicity. The value of Q was given in two ways: as a fixed value $Q=0.5$ and as a linear dependence on the field strength: $Q=3.5\times10^{-5}\Delta V$, simulating electroosmotic flow. Calculations showed that at $\max(|\sigma|,\varepsilon)<0.3$, different assignment of Q leads to negligible quantitative deviation, and choosing equation (21) vs (23) gives results that coincide with graphical accuracy. Below, unless otherwise specified, the solutions of equation (23) at $Q=3.5\times10^{-5}\Delta V$ will be given. Figure 3*a* shows a typical current–voltage characteristic, which for each of the sets of system parameters specified in the legend consists of two straight lines connected by a small transition section. When the system parameters — wall charge, electrolyte flow rate, and Debye number — are changed, the slopes of the straight lines do not change visually, only the transition point between them is shifted. An increase in these parameters leads to a decrease in the transition voltage and vice versa.

It can be stated that the model qualitatively repeats the behavior of an ion-selective membrane. The initial section, obviously, represents the Ohmic (underlimiting) regime; with increasing potential difference the rate of current increase decreases — this corresponds to the limiting regime. For comparison, we give the current–voltage characteristics of model cation-exchange membranes [21] (Fig. 3*b*), where the value N characterizes the selectivity of the membrane

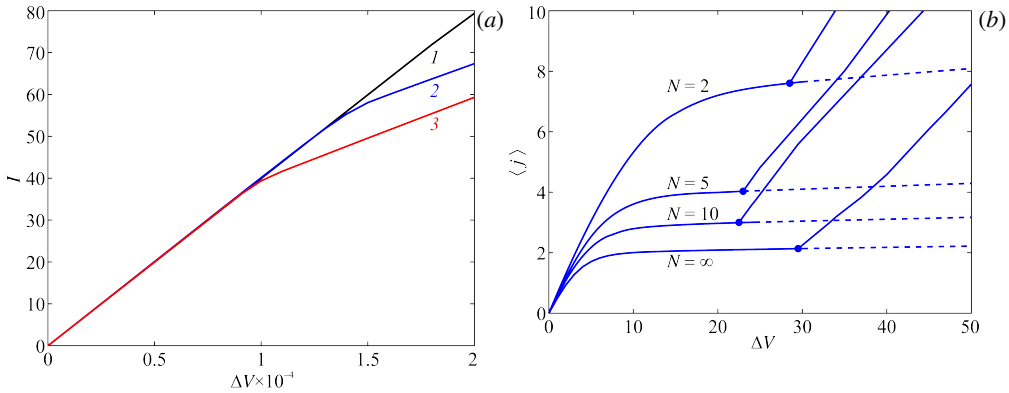

Fig. 3. Current–voltage characteristics of: micro- and nanochannel junction (*a*); partially selective membranes [21] (*b*)

($N = 0$ means a completely unselective surface, and $N = \infty$, a perfectly selective one). The rate of current rise in the limiting regime increases with decreasing selectivity, which agrees well with the assumption of weak selectivity of the considered channel. The absence of an overlimiting regime in the system is also confirmed. Figure 4 shows the profiles of the function $C(x)$ for different regimes at $\varepsilon = 0.3$ and $\sigma = -0.3$ (it corresponds to the plot *3* in Fig. 3*a*). The transition from the underlimiting regime to the limiting regime is characterized by a sharp decrease in the ion concentration and, as a consequence, in the conductivity of the system in the vicinity of the entrance to the nanochannel. Calculations performed for the unsimplified system show qualitatively similar behavior of the total ion concentration and simultaneous growth of the charge density in this region. The obtained results are in qualitative agreement with the results of [15].

The tension $E(x)$ also shows a jump at the junction (see Fig. 5).

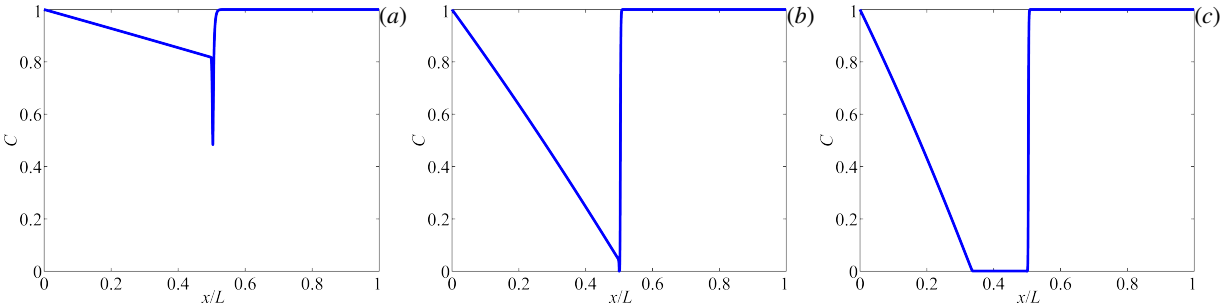

Fig. 4. Change $C(x)$ variation along the channel: underlimiting regime, $\Delta V = 2000$ (*a*); transition to the limiting regime, $\Delta V = 10000$ (*b*); developed limiting regime, $\Delta V = 20000$ (*c*)

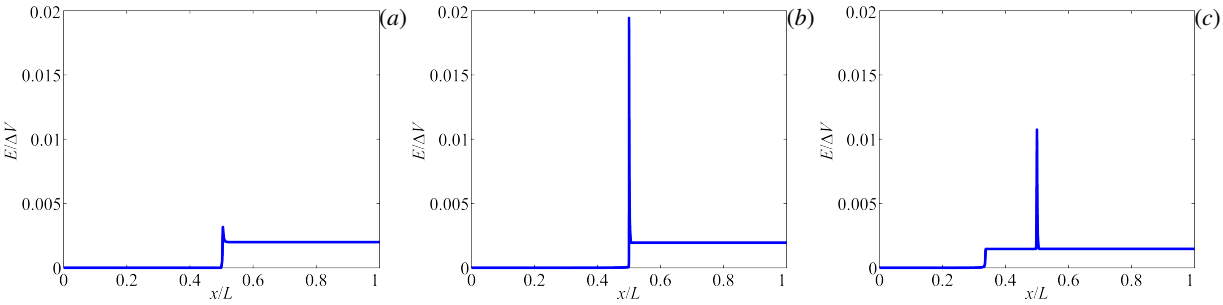

Fig. 5. Variation of $E(x)$ along the channel: underlimiting regime, $\Delta V = 2000$ (*a*); transition to the limiting regime, $\Delta V = 10000$ (*b*); developed limiting regime, $\Delta V = 20000$ (*c*)

The diagram in Figure 6 shows the distribution of the total longitudinal velocity $\mathbf{U}$ and its electroosmotic (U_e) and pressure (U_p) components at different points of the channel. The calculation is performed for equation (21) at zero pressure difference, $\varepsilon = 1$ and $\sigma = -0.1$. For ease of understanding, the transverse coordinate is normalized to the channel thickness:

$\eta = y/H$.

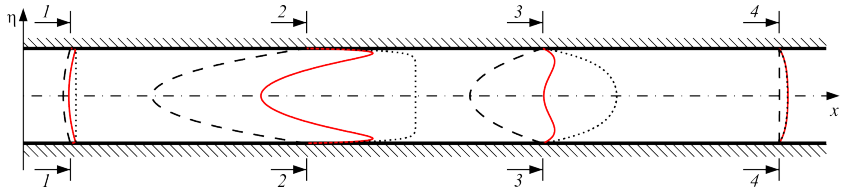

Fig. 6. Schematic representation of velocity profiles at different channel cross-sections: 0.100 (cross-section*1-1*); 0.450 (*2-2*); 0.503 (*3-3*); 0.900 (*4-4*); total velocity is shown as solid line, pressure component, as dashed line, electroosmotic component, as dots

.

Near the inlet (cross-section*1-1*), due to the electroosmotic velocity component, the liquid moves forward and thus resistance is created, which is expressed in the appearance of a negative pressure component $U_p < 0$. The resulting velocity **U** is positive, but there are an inverse flow along the axis of the microchannel and a direct flow near the walls. When approaching the micro- and nanochannel junction (cross-section*2-2*), both electroosmotic and pressure components increase in modulus but maintain their direction. The overall velocity profile suggests vortex formation at this location: this conclusion is consistent with experimental data from [18] and is confirmed by numerical solution of the unsimplified equations. At the entrance to the nanochannel (cross-section*3-3*), both components decrease sharply in modulus but also retain their directions. As the liquid moves to the outlet, the pressure component tends to zero (cross-section*4-4*).

5. Conclusion and discussion

The behavior of dilute electrolyte in a system of joint microchannel and nanochannel with charged walls under the action of pressure and potential difference under the continuum hypothesis was studied numerically. Simplifications based on asymptotic decomposition by a single small parameter, the Debye number or the wall charge density, are used; in the latter case, the model allows consideration of nanochannels whose width is comparable to the thickness of the Debye layer. The main characteristics of the flow and ion distribution are obtained numerically. An analogy between the considered channel and a pore of an ion-exchange membrane is proposed; it is shown that the underlimiting and limiting regimes of membrane operation are also manifested for its individual pore and, therefore, are not a systemic property. The results show satisfactory agreement with the numerical solution of unsimplified equations and experimental data.

The simplified model proposed in this paper allows several important generalizations.

Firstly, as mentioned in Section 3, the wall profile is not limited by the junction of micro- and nanochannel, but can have an arbitrary shape (given by a function of one variable); moreover, the accuracy of the profile depends only on the number of grid cells. As a consequence, the model allows studying nanopores of a given variable cross-section. Presumably, their behavior will also qualitatively look like the behavior of partially-selective membranes — until the transition to the overlimiting regime occurs. This idea is based on the findings of [21], where the qualitative coincidence of the current–voltage characteristics of membranes of different selectivities are shown in the framework of another model. Similarly, the proposed numerical method allows consideration of walls with inhomogeneous charge distribution (the function σ), but the study of the influence of different distributions on the behavior of the system is beyond the scope of the work.

Secondly, consideration of an electrolyte with a larger number of ions can be made by accompanying the equation (1) with similar equations with additional coefficients in the right-hand side (relative diffusion coefficients and charge numbers), while the numerical algorithm remains generally the same both for the simplified formulation and the full one. In particular, the authors have performed preliminary calculations for an electrolyte with suspended strongly charged particles, showing the possibility of controlling the motion of these particles. The model is similarly generalized to the case of flow with dissociation/recombination of ions.

The case of near-zero applied voltage is of a special interest. The violation of electrolyte electroneutrality in the system caused by the wall charge leads to a nonzero electric current in the system and generates a potential difference between the inlet and outlet — the streaming potential (its value is small and is not visible in the graph of figure 3*a* due to the chosen scale). The proposed model shows that the concentration of electrolyte ions at the outlet in such a regime differs from the inlet one and can be both smaller and several times larger. Consideration of this and other effects mentioned above is the subject of a separate study.

This work was supported by the Russian Science Foundation, project No. 22-29-00307 (https://rscf.ru/project/22-29-

00307/).

References

1. *Chang H.-C.*, *Yossifon G.*, *Demekhin E.A.* Nanoscale Electrokinetics and Microvortices: How Microhydrodynamics Affects Nanofluidic Ion Flux. Annual Review of Fluid Mechanics. 2012. Vol. 44. P. 401–426. DOI: 10.1146/annurev-fluid-120710-101046.
2. *Han W.*, *Chen X.* A review: applications of ion transport in micro-nanofluidic systems based on ion concentration polarization. Journal of Chemical Technology & Biotechnology. 2020. Vol. 95. P. 1622–1631. DOI: 10.1002/jctb.6288.
3. *Siwy Z.*, *Gu Y.*, *Spohr H.A.*, *Baur D.*, *Wolf-Reber A.*, *Spohr R.*, *Apel P.*, *Korchev Y.E.* Rectification and voltage gating of ion currents in a nanofabricated pore. Europhysics Letters (EPL). 2002. Vol. 60. P. 349–355. DOI: 10.1209/epl/i2002-00271-3.
4. *Mikhaylin S.*, *Nikonenko V.*, *Pismenskaya N.*, *Pourcelly G.*, *Choi S.*, *Kwon H.J.*, *Han J.*, *Bazinet L.* How physico-chemical and surface properties of cation-exchange membrane affect membrane scaling and electroconvective vortices: Influence on performance of electrodialysis with pulsed electric field. Desalination. 2016. Vol. 393. P. 102–114. DOI: 10.1016/j.desal.2015.09.011.
5. *Levich V.G.* Physicochemical hydrodynamics. New York: Prentice Hall, 1962. 700 p.
6. *Rubinstein I.*, *Zaltzman B.* Electro-osmotically induced convection at a permselective membrane. Physical Review E. 2000. Vol. 62. P. 2238–2251. DOI: 10.1103/PhysRevE.62.2238.
7. *Demekhin E.A.*, *Nikitin N.V.*, *Shelistov V.S.* Direct numerical simulation of electrokinetic instability and transition to chaotic motion. Physics of Fluids. 2013. Vol. 25. 122001. DOI: 10.1063/1.4843095.
8. *Ouyang W.*, *Ye X.*, *Li Z.*, *Han J.* Deciphering ion concentration polarization-based electrokinetic molecular concentration at the micro-nanofluidic interface: theoretical limits and scaling laws. Nanoscale. 2018. Vol. 10. P. 15187–15194. DOI: 10.1039/c8nr02170h.
9. *Abu-Rjal R.*, *Chinaryan V.*, *Bazant M.Z.*, *Rubinstein I.*, *Zaltzman B.* Effect of concentration polarization on permselectivity. Physical Review E. 2014. Vol. 89. 012302. DOI: 10.1103/PhysRevE.89.012302.
10. *Ganchenko G.S.*, *Kalaydin E.N.*, *Schiffbauer J.*, *Demekhin E.A.* Modes of electrokinetic instability for imperfect electric membranes. Physical Review E. 2016. Vol. 94. 063106. DOI: 10.1103/PhysRevE.94.063106.
11. *Demekhin E.A.*, *Ganchenko G.S.*, *Kalaydin E.N.* Transition to electrokinetic instability near imperfect charge-selective membranes. Physics of Fluids. 2018. Vol. 30. 082006. DOI: 10.1063/1.5038960.
12. *Probstein R.F.* Physicochemical Hydrodynamics: An Introduction. Wiley, 1994. 416 p. DOI: 10.1002/0471725137.
13. *Chang H.-C.*, *Yeo L.Y.* Electrokinetically-driven microfluidics and nanofluidics. Cambridge University Press, 2010. 526 p.
14. *Mani A.*, *Zangle T.A.*, *Santiago J.G.* On the Propagation of Concentration Polarization from Microchannel–Nanochannel Interfaces Part I: Analytical Model and Characteristic Analysis. Langmuir. 2009. Vol. 25. P. 3898–3908. DOI: 10.1021/la803317p.
15. *Zangle T.A.*, *Mani A.*, *Santiago J.G.* On the Propagation of Concentration Polarization from Microchannel–Nanochannel Interfaces Part II: Numerical and Experimental Study. Langmuir. 2009. Vol. 25. P. 3909–3916. DOI: 10.1021/la803318e.
16. *Mani A.*, *Bazant M.Z.* Deionization shocks in microstructures. Physical Review E. 2011. Vol. 84. 061504. DOI: 10.1103/PhysRevE.84.061504.
17. *Yaroshchuk A.* Over-limiting currents and deionization "shocks" in current-induced polarization: Local-equilibrium analysis. Advances in Colloid and Interface Science. 2012. Vol. 183/184. P. 68–81. DOI: 10.1016/j.cis.2012.08.004.
18. *Nikonenko V.V.*, *Pismenskaya N.D.*, *Belova E.I.*, *Sistat P.*, *Huguet P.*, *Pourcelly G.*, *Larchet C.* Intensive current transfer in membrane systems: Modelling, mechanisms and application in electrodialysis. Advances in Colloid and Interface Science. 2010. Vol. 160. P. 101–123. DOI: 10.1016/j.cis.2010.08.001.
19. *Schlichting H.* Grenzschicht-Theorie [Boundary layer theory]. G. Braun, 1951. 483 p.
20. *Nikitin N.* Third-order-accurate semi-implicit Runge–Kutta scheme for incompressible Navier–Stokes equations. International Journal for Numerical Methods in Fluids. 2006. Vol. 51. P. 221–233. DOI: 10.1002/fld.1122.
21. *Kiriy V.A.*, *Shelistov V.S.*, *Kalaidin E.N.*, *Demekhin E.A.* Hydrodynamics, electroosmosis, and electrokinetic instability in imperfect electric membranes. Doklady Physics. 2017. Vol. 62. P. 222–227. DOI: 10.1134/s1028335817040139.

Authors' Details:

Alekseev Maxim Sergeyevich; e-mail: MrMaxnhbyflwfnm@mail.ru; ORCID: 0009-0007-3011-1560

Ponomarev Roman Rostislavovich; e-mail: stivepro@gmail.com; ORCID: 0009-0004-3269-6580

Shelistov Vladimir Sergeyevich (corr.); e-mail: VSShelistov@fa.ru; ORCID: 0009-0001-1142-9801

Popov Vladislav Anatolievich; e-mail: Vladislav.11.ru@yandex.ru; ORCID: 0009-0001-4758-9129
Morshneva Irina Viktorovna; e-mail: morsh4@yandex.ru; ORCID: 0009-0000-6784-146X
Demekhin Evgeny Afanasyevich; e-mail: edemekhi@gmail.com; ORCID: 0009-0001-6280-7171